Synthesis and Photocatalytic Properties of Hollow Microparticles of Titania and Titania/Carbon Composites Templated by Sephadex G-100

Dayong Zhang, Dong Yang, Huijuan Zhang, Conghua Lu, and Limin Qi*

Beijing National Laboratory for Molecular Sciences (BNLMS), State Key Laboratory for Structural Chemistry of Unstable and Stable Species, College of Chemistry, Peking University, Beijing 100871, People's Republic of China

Received March 2, 2006. Revised Manuscript Received May 23, 2006

Hollow titania microparticles about 20−60 μm in size and hollow titania/carbon composite microparticles about 30−90 μm in size were prepared by employing commercial Sephadex G-100 beads as the template as well as the carbon precursor. The cross-linked dextran gel template was first immersed in aqueous $TiCl_4$ solution to allow the surface mineralization of titania, resulting in the formation of hollow microparticles of titania/G-100 hybrids. Hollow titania microparticles with a shell thickness adjustable from 1 μm to 2.5 μm were fabricated by calcination of the hollow titania/G-100 hybrid microparticles at temperatures from 400 to 700 °C in air. On the other hand, hollow titania/carbon composite microparticles $\sim$ 2.6 μm in shell thickness, which consisted of anatase nanocrystals and amorphous carbon, were obtained by carbonization of the hollow titania/G-100 hybrid microparticles at temperatures from 500 to 700 °C in flowing nitrogen. For the titania/carbon composites, the phase transformation from anatase to rutile was suppressed; moreover, the crystallinity of anatase was decreased and the surface area was increased with increasing calcination temperature, in contrast to the case of hollow titania microparticles. The photocatalytic activity of the obtained hollow microparticles of titania and titania/carbon composites was investigated by monitoring the photodegradation of Rhodamine B. In both cases, the product calcined at an intermediate temperature exhibited the highest photocatalytic activity possibly because of a compromise between the anatase crystallinity and the surface area. Compared with the hollow titania microparticles, the hollow titania/carbon composite microparticles exhibit remarkably enhanced photocatalytic activity.

Introduction

Inorganic hollow structures have attracted great attention because of their wide variety of potential applications as catalysts and catalyst supports, adsorbents, sensors, drug-delivery carriers, artificial cells, photonic crystals, acoustic insulators, lightweight fillers, and microreactors.[1,2] In particular, many recent efforts have been devoted to the controlled fabrication of hollow TiO_2 particles because titania is an important semiconductor material applicable in various areas including photovoltaics, photocatalysis, separation, chemical sensing, and optical devices. While hollow TiO_2 particles have been synthesized without the assistance of templates by the spray-drying technique[3] and via Ostwald ripening,[4] the templating method has been most frequently used for the synthesis of hollow TiO_2 particles with tailored properties. For example, colloidal polymer spheres have been used as sacrificial hard templates for the fabrication of hollow titania spheres with controlled shell thickness and cavity size through sol−gel coating[5] and the layer-by-layer (LbL) technique[6] whereas emulsion droplets have been used as easily removable soft templates for the interfacial synthesis of hollow microspheres of TiO_2,[7] porous TiO_2,[8] and TiO_2/CdS composites.[9] Generally, the structural parameters of hollow TiO_2 particles can be better controlled by the hard template route; however, the currently employed polymer particles as well as the templated hollow TiO_2 particles are normally less than 10 μm. It would be desirable to find suitable colloidal hard templates to achieve size control for relatively large hollow TiO_2 microparticles of sizes about

* To whom correspondence should be addressed. E-mail: liminqi@pku.edu.cn.

(1) (a) Caruso, F. *Chem.—Eur. J.* **2000**, *6*, 413. (b) Sun, Y.; Mayers, B.; Xia, Y. *Adv. Mater.* **2003**, *15*, 641. (c) Kim, S.-W.; Kim, M.; Lee, W. Y.; Hyeon, T. *J. Am. Chem. Soc.* **2002**, *124*, 7642. (d) Yin, Y.; Rioux, R. M.; Erdonmez, C. K.; Hughes, S.; Somorjai, G. A.; Alivisatos, A. P. *Science* **2004**, *304*, 711.

(2) (a) Qi, L.; Li, J.; Ma, J. *Adv. Mater.* **2002**, *14*, 300. (b) Zhang, D.; Qi, L.; Ma, J.; Cheng, H. *Adv. Mater.* **2002**, *14*, 1499. (c) Ma, Y.; Qi, L.; Ma, J.; Cheng, H. *Langmuir* **2003**, *19*, 4040. (d) Yang, J.; Qi, L.; Lu, C.; Ma, J.; Cheng, H. *Angew. Chem., Int. Ed.* **2005**, *44*, 598. (e) Lu, C.; Qi, L.; Yang, J.; Wang, X.; Zhang, D.; Xie, J.; Ma, J. *Adv. Mater.* **2005**, *17*, 2562.

(3) Iida, M.; Sasaki, T.; Watanabe, M. *Chem. Mater.* **1998**, *10*, 3780.

(4) (a) Yang, H. G.; Zeng, H C. *J. Phys. Chem. B* **2004**, *108*, 3492. (b) Li, J.; Zeng, H. C. *Angew. Chem., Int. Ed.* **2005**, *44*, 4342.

(5) (a) Zhong, Z.; Yin, Y.; Gates, B.; Xia, Y. *Adv. Mater.* **2000**, *12*, 206. (b) Yang, Z.; Niu, Z.; Lu, Y.; Hu, Z.; Han, C. C. *Angew. Chem., Int. Ed.* **2003**, *42*, 1943.

(6) (a) Caruso, F.; Shi, X.; Caruso, R. A.; Susha, A. *Adv. Mater.* **2001**, *13*, 740. (b) Caruso, R. A.; Susha, A.; Caruso, F. *Chem. Mater.* **2001**, *13*, 400. (c) Wang, L.; Sasaki, T.; Ebina, Y.; Kurashima, K.; Watanabe, M. *Chem. Mater.* **2002**, *14*, 4827.

(7) (a) Collins, A. M.; Spickermann, C.; Mann, S. *J. Mater. Chem.* **2003**, *13*, 1112. (b) Nakashima, T.; Kimizuka, N. *J. Am. Chem. Soc.* **2003**, *125*, 6386.

(8) (a) Ren, T.-Z.; Yuan, Z.-Y.; Su, B.-L. *Chem. Phys. Lett.* **2003**, *374*, 170. (b) Strohm, H.; Löbmann, P. *J. Mater. Chem.* **2004**, *14*, 2667.

(9) Hu, J.-S.; Guo, Y.-G.; Liang, H.-P.; Wan, L.-J.; Bai, C.-L.; Wang, Y.-G. *J. Phys. Chem. B* **2004**, *108*, 9734.

10.1021/cm060503p CCC: $33.50
Published on Web 07/01/2006

tens of micrometers considering that these microparticles could open new possibilities for the applications as packing materials in chromatography as well as lightweight fillers or as an easy-to-handle form for catalytic purposes.

Because of the widespread applications of carbon materials (e.g., amorphous carbon, activated carbon, and graphite) as absorbents, catalyst supports, nanocomposites, electrode materials, and storage media,[10] considerable attention has been paid to the fabrication of hollow carbon particles through carbonization of carbon precursors[11] and chemical vapor deposition.[12] Interestingly, hollow spheres of mesoporous carbon have been employed as templates to fabricate hollow spheres of crystalline porous metal oxides, such as hollow porous TiO_2 microspheres of size between 2 and 5 μm.[13] It is noteworthy that there has been increasing interest in titania/carbon composites in recent years. It has been demonstrated that carbon doping can dramatically improve the photocatalytic activity of titania in the visible-light region.[14] Titania-mounted activated carbon has been prepared with the advantage of coupling the photoactivity of anatase-type TiO_2 with the adsorptivity of activated carbon[15] whereas carbon-coated titania has been found to show many advantages such as stabilization of the anatase phase, shift of the absorption edge of titania to the visible region, and high photocatalytic activity.[16] Recently, three-dimensionally ordered macroporous (3DOM) carbon/titania nanoparticle composites with potential applications in sensing, photocatalysis, and sorption have been synthesized by coating TiO_2 nanoparticles onto prefabricated 3DOM carbon.[17] However, hollow particles of titania/carbon composites, which combine the unique structure of hollow particles and the useful properties of titania/carbon composites, have not been reported so far although there has been some work on the preparation of titania/carbon composite microparticles.[18] Hence, it remains a challenge to explore effective methods to synthesize hollow titania/carbon composite particles with tailored properties.

A variety of structured organic templates have been employed to synthesize titania materials with controlled morphologies and microstructures because template-directed synthesis represents an ideal approach to replication by the design and fabrication of materials with predetermined structural properties.[19] In this regard, synthetic polymer gels,[20] porous polymer beads,[21] and electrospun polymer fibers[22] have been used for the synthesis of porous TiO_2 networks, porous TiO_2 spheres, and TiO_2 tubes, respectively, while cellulose acetate membranes have been employed to prepare porous TiO_2 films.[23] Moreover, biological structures such as eggshell membranes,[24] bacterial cellulose membranes,[25] and natural cellulose matrixes (e.g., filter paper, cloth, and cotton)[26] have be adopted as delicate biological templates to replicate porous TiO_2 networks or hierarchical TiO_2 structures. Sephadex gels are a group of cross-linked dextran gels widely used in gel filtration for separation, purification, and molecular weight determination of biomacromolecules including proteins and polysaccharides.[27] In particular, Sephadex G-100 is a dextran gel that considerably swells in water with a water regain of 10 g per g dry gels, and it is relatively stable in both basic and acidic environments. Commercial Sephadex G-100 beads are normally prepared by suspension polymerization of low molecular weight dextran with epichlorohydrin as the cross-linker and are frequently used in gel filtration for proteins ranging from 200 to 1.2×10^6 in the molecular weight.[28] Sephadex G-100 beads are actually hollow microspheres of dextran gels, which are potential templates for inorganic hollow particles and provide suitable precursors for carbonization because dextran is a polysaccharide composed of repeated monomeric glucose units with a predominance of α-1,6-linkages. In the present work, Sephadex G-100 beads are used as both templates and carbon precursors for the controlled synthesis of large hollow titania microparticles and unique hollow titania/carbon composite microparticles. Compared with the hollow titania microparticles, the hollow titania/carbon composite microparticles exhibit remarkably enhanced photocatalytic activity.

(10) (a) Sakintuna, B.; Yürüm, Y. *Ind. Eng. Chem. Res.* **2005**, *44*, 2893. (b) Yoon, S. B.; Chai, G. S.; Kang, S. K.; Yu, J.-S.; Gierszal, K. P.; Jaroniec, M. *J. Am. Chem. Soc.* **2005**, *127*, 4188. (c) Lee, K. T.; Lytle, J. C.; Ergang, N. S.; Oh, S. M.; Stein, A. *Adv. Funct. Mater.* **2005**, *15*, 547. (d) Luo, T.; Gao, L.; Liu, J.; Chen, L.; Shen, J.; Wang, L.; Qian, Y. *J. Phys. Chem. B* **2005**, *109*, 15272.

(11) (a) Yoon, S. B.; Sohn, K.; Kim, J. Y.; Shin, C.-H.; Yu, J.-S.; Hyeon, T. *Adv. Mater.* **2002**, *14*, 19. (b) Han, S.; Yun, Y.; Park, K.-W.; Sung, Y.-E.; Hyeon, T. *Adv. Mater.* **2003**, *15*, 1922. (c) Herring, A. M.; McKinnon, J. M.; McCloskey, B. D.; Filley, J.; Gneshin, K. W.; Pavelka, R. A.; Kleebe, H.-J.; Aldrich, D. J. *J. Am. Chem. Soc.* **2003**, *125*, 9916.

(12) (a) Xia, Y.; Mokaya, R. *Adv. Mater.* **2004**, *16*, 886. (b) Xia, Y.; Yang, Z.; Mokaya, R. *J. Phys. Chem. B* **2004**, *108*, 19293. (c) Wang, Y.; Su, F.; Lee, J. Y.; Zhao, X. S. *Chem. Mater.* **2006**, *18*, 1347.

(13) Xia, Y.; Mokaya, R. *J. Mater. Chem.* **2005**, *15*, 3126.

(14) (a) Khan, S. U. M.; Al-Shahry, M.; Ingler, W. B., Jr. *Science* **2002**, *297*, 2243. (b) Sakthivel, S.; Kisch, H. *Angew. Chem., Int. Ed.* **2003**, *42*, 4908. (c) Neumann, B.; Bogdanoff, P.; Tributsch, H.; Sakthivel, S.; Kisch, H. *J. Phys. Chem. B* **2005**, *109*, 16579. (d) Valentin, C. D.; Pacchioni, G.; Selloni, A. *Chem. Mater.* **2005**, *17*, 6656.

(15) Tryba, B.; Morawski, A. W.; Inagaki, M. *Appl. Catal. B* **2003**, *41*, 427.

(16) (a) Inagaki, M.; Kojin, F.; Tryba, B.; Toyoda, M. *Carbon* **2005**, *43*, 1652. (b) Lin, L.; Lin, W.; Zhu, Y. X.; Zhao, B. Y.; Xie, Y. C.; He, Y.; Zhu, Y. F. *J. Mol. Catal. A* **2005**, *236*, 46.

(17) Wang, Z.; Ergang, N. S.; Al-Daous, M. A.; Stein, A. *Chem. Mater.* **2005**, *17*, 6805.

(18) Nagaoka, S.; Hamasaki, Y.; Ishihara, S.; Nagata, M.; Iio, K.; Nagasawa, C.; Ihara, H. *J. Mol. Catal. A* **2002**, *177*, 255.

(19) Caruso, R. A. *Angew. Chem., Int. Ed.* **2004**, *43*, 2746.

(20) (a) Caruso, R. A.; Giersig, M.; Willig, F.; Antonietti, M. *Langmuir* **1998**, *14*, 6333. (b) Caruso, R. A.; Antonietti, M.; Giersig, M.; Hentze, H.-P.; Jia, J. *Chem. Mater.* **2001**, *13*, 1114. (c) Schattka, J. H.; Shchukin, D. C.; Jia, J.; Antonietti, M.; Caruso, R. A. *Chem. Mater.* **2002**, *14*, 5103. (d) Schukin, D. G.; Schattka, J. H.; Antonietti, M.; Caruso, R. A. *J. Phys. Chem. B* **2003**, *107*, 952.

(21) (a) Meyer, U.; Larsson, A.; Hentze, H. P.; Caruso, R. A. *Adv. Mater.* **2002**, *14*, 1768. (b) Shchukin, D. G.; Caruso, R. A. *Chem. Mater.* **2004**, *16*, 2287. (c) Deshpande, A. S.; Shchukin, D. G.; Ustinovich, E.; Antonietti, M.; Caruso, R. A. *Adv. Funct. Mater.* **2005**, *15*, 239. (d) Zhang, H.; Hardy, G. C.; Khimyak, Y. Z.; Rosseinsky, M. J.; Cooper, A. I. *Chem. Mater.* **2004**, *16*, 4245.

(22) Caruso, R. A.; Schattka, J. H.; Greiner, A. *Adv. Mater.* **2001**, *13*, 1577.

(23) (a) Caruso, R. A.; Schattka, J. H. *Adv. Mater.* **2000**, *12*, 1921. (b) Shchukin, D. G.; Caruso, R. A. *Adv. Funct. Mater.* **2003**, *13*, 789.

(24) Yang, D.; Qi, L.; Ma, J. *Adv. Mater.* **2002**, *14*, 1543.

(25) Zhang, D.; Qi, L. *Chem. Commun.* **2005**, 2735.

(26) Huang, J.; Kunitake, T. *J. Am. Chem. Soc.* **2003**, *125*, 11834.

(27) Flodin P. *Polym. Eng. Sci.* **1998**, *38*, 1220.

(28) (a) Ni, X.; Hager, L. P. *Proc. Natl. Acad. Sci. U.S.A.* **1998**, *95*, 12866. (b) Chacko, B. K.; Appukuttan, P. S. *Mol. Immunol.* **2003**, *39*, 933. (c) Lee, S.-C.; Whitaker, J. R. *J. Agric. Food Chem.* **2004**, *52*, 4948. (d) Leite, K.; Tadiotti, A.; Baldochi, D.; Oliveira, O. *Food Chem.* **2006**, *94*, 565.

Experimental Section

Materials. Sephadex G-100 beads with the dry diameter about 40−120 μm were obtained from Amersham Biosciences (Uppsala, Sweden). $TiCl_4$ and ethanol were of analytical grade. All the chemicals were used as received, and the water used was deionized.

Synthesis. A stock $TiCl_4$ solution (2.6 M) was prepared by dropping $TiCl_4$ into water at 0 °C under vigorous stirring, which was diluted to 0.1 M just prior to the templating synthesis. Sephadex G-100 beads were immersed in hot water (~80 °C) for 8 h to swell thoroughly, which was followed by separation of the swollen beads by filtration. Then, the swollen Sephadex G-100 beads (2 g) were added to 20 mL of 0.1 M $TiCl_4$ solution at room temperature and the suspension was stirred for 8 h unless otherwise stated. After the mineralized beads sedimented on the bottom of the beaker, the upper clear solution was carefully decanted and ethanol was added to wash the beads under stirring, which resulted in a considerable shrinkage of the swollen beads due to the extraction of the adsorbed water accompanying an apparent change of the solids from translucent to a white color. The washing process was repeated for several times, and the resultant titania/G-100 hybrids were recovered by filtration and dried in air at 60 °C. The obtained titania/G-100 hybrids were further calcined at different temperatures (with a heating rate of 200 °C/h) for 3 h under air or nitrogen atmosphere to burn off or carbonize the dextrans, resulting in the formation of hollow titania microparticles or hollow titania/carbon composite microparticles, respectively.

Characterization. Optical microscopy (OM) images were recorded on a Nikon ECLIPSE E600 microscope. Environmental scanning electron microscopy (SEM) images were taken on a FEI Quanta 200FEG microscope at an accelerating voltage of 15 kV with the pressure in the sample chamber of 1 Torr. Conventional transmission electron microscopy (TEM) and high-resolution transmission electron microscopy (HRTEM) images were recorded on a JEOL JEM-200CX microscope at 160 kV, and a FEI TECNAI F30 microscope at 300 kV, respectively. X-ray diffraction (XRD) was performed on a Rigaku Dmax-2000 X-ray diffractometer with Cu Kα radiation. Thermogravimetric analysis (TGA) was carried out on a SDT 2960 (Thermal Analysis, U.S.A.) with the carrier gas of air or N_2 at a heating rate of 10 °C min^{-1}. Specific surface areas were measured on a Micromeritics ASAP 2010 analyzer using BET analysis based on N_2 adsorption at 77 K. Raman spectra were obtained from Renishaw micro-Raman 1000 spectrometer with a 50 mW He−Ne laser operating at 632.8 nm.

Photocatalytic Activity Measurements. The photocatalytic activity of the obtained hollow microparticles of titania and titania/carbon composites was characterized by measuring the titania-assisted photodegradation of the xanthene dye Rhodamine B, following the reported procedure.[25] The hollow microparticles (10 mg for titania samples and 20 mg for titania/carbon composites) were suspended in 100 mL of 0.01 mM aqueous Rhodamine B, and the suspensions were placed in the dark for 30 min before illumination to allow sufficient adsorption of Rhodamine B. The stirred suspensions were illuminated with a 250 W high-pressure mercury lamp ~ 25 cm high over the solution, and the change of the Rhodamine B concentration with irradiation time was monitored by measuring the UV−vis absorption of the suspensions centrifuged at 2000 rpm to remove titania-containing microparticles at different interval periods. The UV−vis absorption was measured on a CARY 1E spectrometer, and the absorbance at the absorption maximum (553 nm) was used for the determination of the concentration of Rhodamine B.

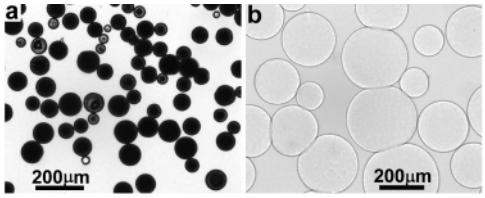

Figure 1. OM images of Sephadex G-100 beads before (a) and after (b) swelling in water.

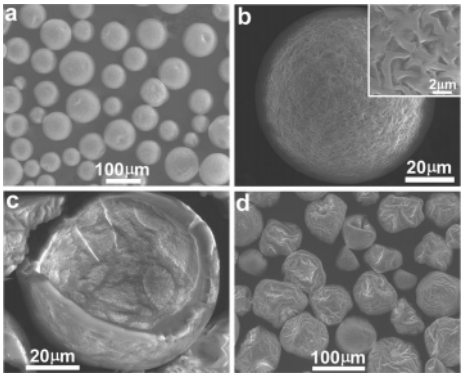

Figure 2. SEM images of dry Sephadex G-100 beads as received (a, b) and after being manually broken (c). (d) SEM image of Sephadex G-100 beads re-dried by extracting water with ethanol and drying in air after swolling in water.

Results and Discussion

Hollow Titania/G-100 Hybrid Microparticles. Sephadex G-100 is a relatively loosely cross-linked dextran gel with a large water regain of 10 g/g. The as-received Sephadex G-100 beads swelled significantly in water whereas they almost kept their original sizes when they were suspended in ethanol because they did not tend to absorb ethanol. A representative OM image of the dry Sephadex G-100 beads suspended in ethanol is presented in Figure 1a, which suggests that the beads are perfect spheres ranging in size from 40 to 120 μm. Although it is hard to see any inner structures for the larger spheres, the smaller spheres usually show a dark edge and a pale center, indicating a hollow structure. Figure 1b shows a typical OM image of the swollen Sephadex G-100 beads suspended in water, which exhibit spheres about 100−350 μm in diameter, much larger than the dry beads. It can be seen that the contrast between these spheres and the background is rather low as a result of the encapsulation of a large amount of water in the gel networks, and it is now difficult to see the hollow structure. Environmental SEM was conducted to reveal the detailed morphological characteristics of the original dry Sephadex G-100 beads as well as the re-dried Sephadex G-100 beads after swelling in water (Figure 2). As shown in Figure 2a,b, the original gel beads are spherical particles 40−120 μm in diameter with their surface full of micrometer-sized wrinkles. The Sephadex G-100 beads can be manually broken by grinding, and a typical SEM image shown in Figure 2c clearly reveals that the microspheres are actually hollow spheres with a shell thickness about 4.5 μm. When the Sephadex G-100 beads thoroughly swollen in water were re-dried by repeatedly extracting water with ethanol and drying in air, the resultant hollow microparticles nearly shrank back to their original sizes, but they were apparently deformed with some obvious sinkage in addition to the

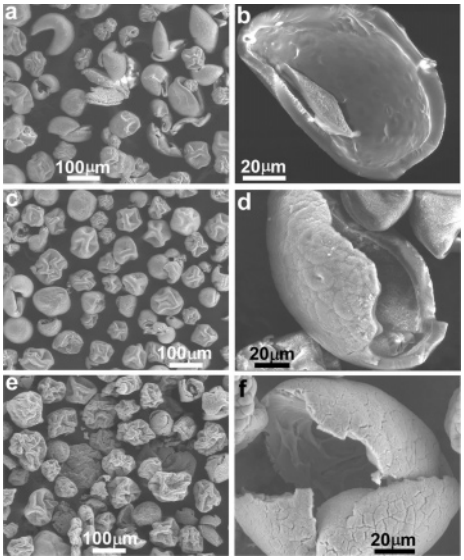

Figure 3. SEM images of titania/G-100 hybrids obtained after different reaction times: (a, b) 2 h, (c, d) 8 h, and (e, f) 24 h.

surface wrinkles (Figure 2d). Such a reversible process of swelling in water and shrinking in ethanol may indicate the potential application of the elastic Sephadex G-100 beads in the templating synthesis of inorganic hollow microparticles since the swelling may allow the easy infiltration of precursors and the shrinking may allow the entanglement of the mineralized solids.

When the swollen Sephadex G-100 beads were immersed in a 0.1 M $TiCl_4$ solution, the hydrolysis of $TiCl_4$ would occur preferentially on the surface of the cross-linked dextran chains because their surface hydroxyl groups could interact with the intermediate titanium species such as $[Ti(OH)_nCl_m]^{2-}$ where $n + m = 6$.[29] Actually, the hydrolysis of $TiCl_4$ on and inside the G-100 beads started immediately after the G-100 beads were immersed while the hydrolysis in the $TiCl_4$ solution without the G-100 beads was very slow and no precipitates were observed after 24 h of aging. It indicated that the surface hydroxyl groups of the dextran chains could instigate the $TiCl_4$ hydrolysis in the current situation. After titania mineralization followed by washing with ethanol and drying in air, titania/G-100 hybrids were obtained, which are shown in Figure 3. It can be seen that the titania/G-100 hybrids obtained with reaction times ranging from 2 to 24 h are all shrunken hollow microparticles with their overall morphology, size, and shell thickness similar to the re-dried hollow Sephadex G-100 microparticles shown in Figure 2d. This result suggests that $TiCl_4$ diffused into the macroporous networks of the swollen gels and then hydrolyzed on the cross-linked dextran chains, resulting in the formation of titania-coated gel networks. After dehydrating with ethanol and drying, the swollen gels shrank into deformed microspheres with mineralized titania enwrapped inside the condensed gel networks, leading to the formation of the hollow titania/G-100 hybrid microparticles that look like the re-dried hollow Sephadex G-100 microparticles. Figure 4 shows the TGA curve of the titania/G-100 hybrids obtained with a reaction time of 8 h, which suggests that organics

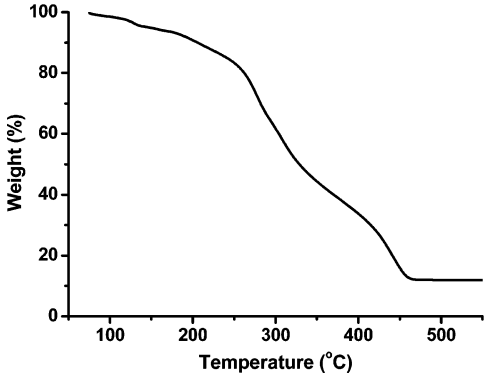

Figure 4. TGA curve of the titania/G-100 hybrid obtained after 8 h of reaction and heating in air.

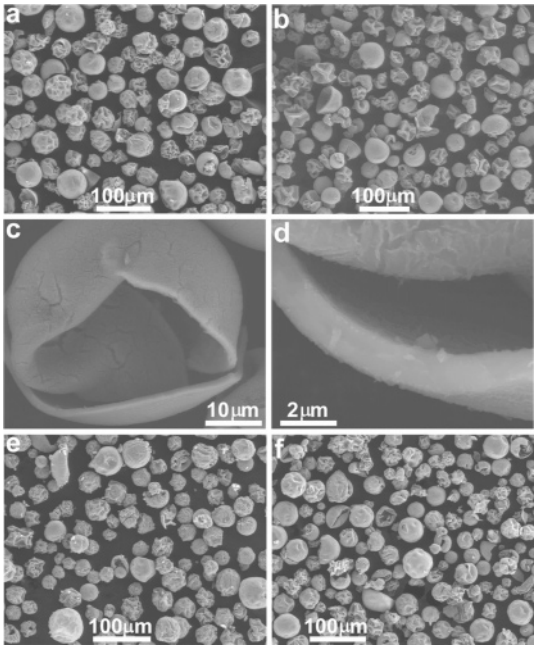

Figure 5. SEM images of hollow titania microparticles obtained after reaction for 8 h and calcination in air at different temperatures: (a) 400 °C, (b−d) 500 °C, (e) 600 °C, and (f) 700 °C.

were burnt off around 470 °C, leaving 12 wt % inorganic solid. On the basis of the TGA measurements, it was estimated that the titania content in the titania/G-100 hybrids was increased from 6.5 to 37 wt % with increasing reaction time from 2 to 24 h, indicating a gradual deposition of titania on the gel networks with reaction time. It can also be seen from Figure 3 that broken entities are rather common in the hybrid particles obtained after 2 h of reaction while the hybrid particles obtained after longer time exist mostly as intact particles, which may indicate that the strength of the hybrid wall with a small content of titania could be too low to withstand the shrinking force. Moreover, some surface cracking is evident in the hybrid particles obtained after 24 h of reaction (Figure 3f), which could partly be attributed to the deposition of extra titania on the surface of the G-100 beads.

Hollow Titania Microparticles. Calcination of the hollow titania/G-100 hybrid microparticles in air resulted in the formation of hollow titania microparticles. Figure 5 displays the SEM images of hollow titania microparticles obtained after reaction for 8 h and calcination in air at different temperatures. It shows that all the obtained titania products

(29) Cheng, H.; Ma, J.; Zhao, Z.; Qi, L. *Chem. Mater.* **1995**, *7*, 663.

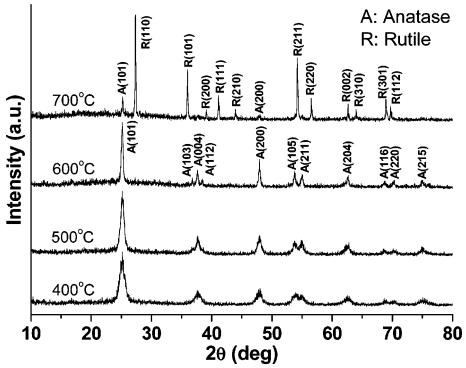

Figure 6. XRD patterns of hollow titania microparticles obtained after reaction for 8 h and calcination in air at different temperatures.

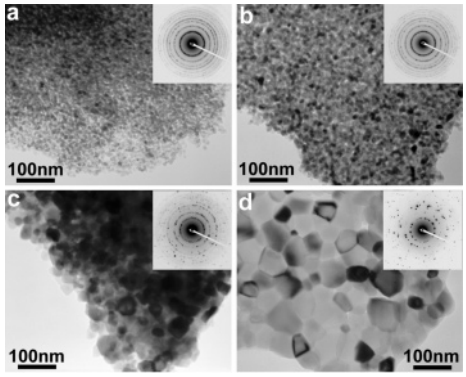

Figure 7. TEM images of hollow titania microparticles obtained after reaction for 8 h and calcination in air at different temperatures: (a) 400 °C, (b) 500 °C, (c) 600 °C, and (d) 700 °C.

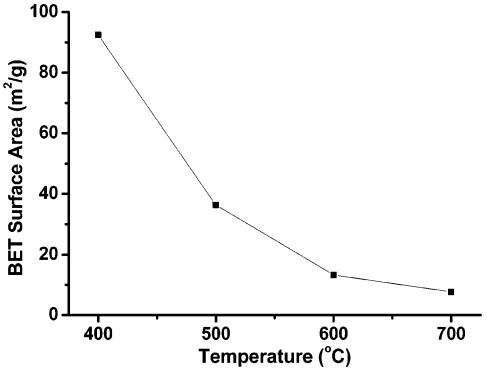

Figure 8. Variation of BET surface area of hollow titania microparticles versus calcination temperature.

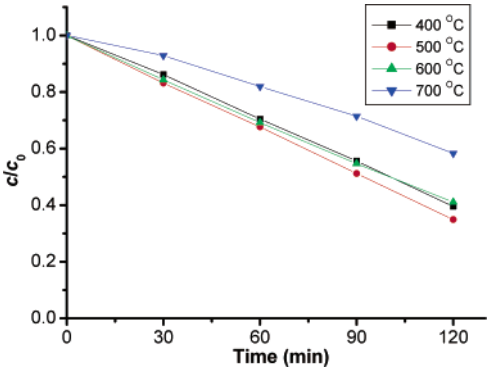

Figure 9. Photodegradation of Rhodamine B monitored as the normalized concentration change versus irradiation time in the presence of hollow titania microparticles obtained after reaction for 8 h and calcination in air at different temperatures.

are similar shrunken hollow microparticles with sizes predominantly in the range 20−60 μm, considerably smaller than the parent hollow microparticles of titania/G-100 hybrids (around 40−120 μm). Representative high-magnification images of the broken samples calcined at 500 °C suggest that the hollow titania microparticles with surface wrinkles have a condensed shell with a shell thickness ∼ 1.5 μm (Figure 5c,d). Our preliminary density measurement revealed that the hollow titania microparticles calcined at 500 °C had a density ∼ 3.0 g cm^{-3}, which is considerably lower that the density of the normal titania powders (∼4.2 g cm^{-3}). The XRD patterns of the hollow titania microparticles are presented in Figure 6, which reveals that the titania existed in the crystal phase of anatase when heated at temperatures 400−600 °C, and the transformation to the rutile structure occurred at 700 °C with the rutile phase existing as the predominant crystal phase. According to the line width analysis of the (101) reflection based on the Scherrer formula, average crystallite sizes for the hollow anatase microparticles obtained at 400, 500, and 600 °C were estimated to be about 8, 12, and 28 nm, respectively.

Figure 7 presents typical TEM images of the hollow titania microparticles along with the related electron diffraction patterns. It shows that the products obtained at 400−600 °C consist of anatase nanocrystals, the crystallite size of which increases from less than 10 nm to larger than 20 nm with increasing temperature from 400 to 600 °C, and the product obtained at 700 °C mainly comprises large rutile nanocrystals (mostly 40−90 nm), in good agreement with the XRD result. Furthermore, the variation of the BET specific surface area of the hollow titania microparticles versus calcination temperature is displayed in Figure 8, which clearly shows that the surface area monotonically decreases from 92 to 7.7 m^2 g^{-1} with increasing temperature from 400 to 700 °C. To summarize, for the hollow titania microparticles, an increase in the calcination temperature results in an increase in the crystallite size, which is accompanied by a phase transformation from anatase to rutile around 700 °C, and a decrease in the surface area, while the apparent morphology of the hollow particles remains unchanged.

The photocatalytic activity of the hollow titania microparticles obtained at different temperatures was examined by measuring the photodegradation of Rhodamine B in an aqueous suspension of the titania photocatalyst with a concentration of 0.1 g L^{-1}. As shown in Figure 9, the sample heated at 700 °C exhibits the lowest photocatalytic activity, and the samples calcined at 400−600 °C show comparable photocatalytic activity with the sample at 500 °C exhibiting the highest activity. The lowest photocatalytic activity for the sample heated at 700 °C may be attributed to the low surface area and the crystal phase of rutile because the anatase-type titania usually shows higher photocatalytic activity than the rutile-type titania. For the anatase samples obtained at 400−600 °C, the crystallinity and the surface area seem to be the two important factors in determining the photocatalytic activity. In general, the photocatalytic activity of anatase increases with the crystallinity and the surface area. Therefore, the highest photocatalytic activity of the sample obtained at 500 °C could result from a compromise between the crystallinity and the surface area

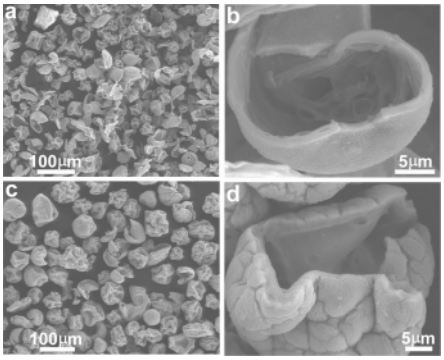

Figure 10. SEM images of hollow titania microparticles obtained after reaction for 2 h (a, b) and 24 h (c, d) followed by calcination at 500 °C in air.

as the crystallinity increases, but the surface area decreases with increasing calcination temperature. It is worth noting that the photocatalytic activity of the current hollow titania microparticles obtained at 500 °C is actually comparable to the photocatalytic activity of the mesoporous titania networks templated by bacterial cellulose membranes.[25] Considering that the hollow titania microparticles (~20−60 μm) can be easily suspended in and recovered from solution, they may find some promising applications including as catalysts and lightweight fillers.

In addition, the shell thickness of the hollow titania microparticles can be adjusted readily by varying the reaction time between the gel beads and $TiCl_4$ in water. Figure 10 shows the SEM images of the hollow titania microparticles obtained with a shorter and a longer reaction time, that is, 2 and 24 h, which suggests that they have shell thicknesses about 1 μm and 2.5 μm, respectively. It can be also observed that a large portion of the hollow microparticles with a reaction time of 2 h exist as broken fragments due to the relatively thin shell of the hollow microparticles (Figure 10a), in contrast to the hollow microparticles with a longer reaction time, which exist mostly in intact shrunken microparticles as in Figures 5 and 10c. Although the parent titania/G-100 hybrid microparticles with different reaction times exhibit a similar shell thickness (Figure 3), the titania content in the hybrids increases with increasing reaction time, which may lead to a thicker shell for the calcined hollow microparticles with a longer reaction time.

Hollow Titania/Carbon Composite Microparticles. Calcination of the hollow titania/G-100 hybrid microparticles in flowing N_2 led to the carbonization of cross-linked dextrans and incorporation of deposited titania, resulting in the formation of hollow microparticles of titania/carbon composites. As shown in Figure 11, the titania/G-100 hybrid obtained after 8 h of reaction starts pyrolysis under N_2 around 180 °C, and the pyrolysis process continues until more than 800 °C; however, there is still a small weight loss when the heating temperature is higher than 500 °C. Figure 12 shows representative SEM images of the hollow titania/carbon composite microparticles obtained after 3 h of carbonization in N_2 at different temperatures. The obtained composite microparticles exhibit shrunken hollow spheres of sizes predominantly in the range 30−90 μm, which are essentially smaller than the parent hollow titania/G-100 hybrid microparticles (40−120 μm) but larger than the templated hollow

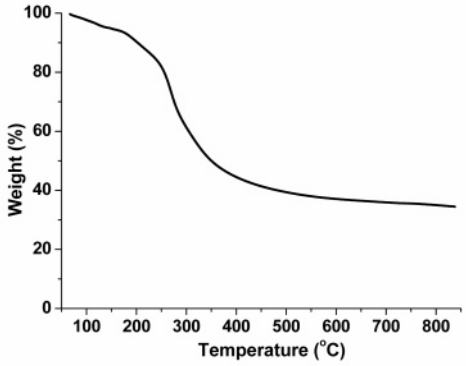

Figure 11. TGA curve of titania/G-100 hybrid obtained after 8 h of reaction and being pyrolyzed in N_2.

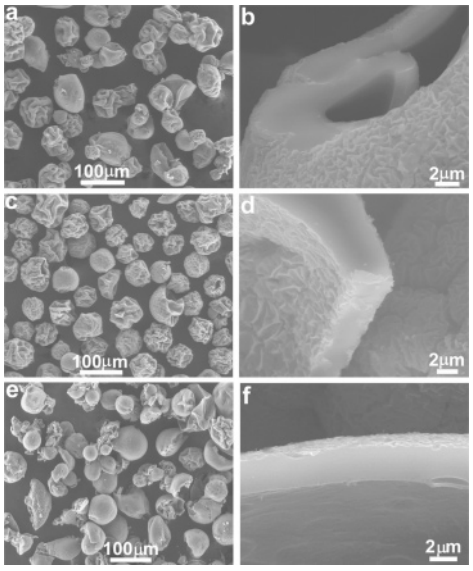

Figure 12. SEM images of hollow titania/carbon composite microparticles pyrolyzed in N_2 at different temperatures: (a, b) 500 °C, (c, d) 600 °C, and (e, f) 700 °C.

Table 1. Titania Content and BET Surface Area of the Hollow Titania/Carbon Composite Microparticles Pyrolyzed at Different Temperatures

pyrolysis temperature (°C)	titania content (wt %)	BET surface area ($m^2\ g^{-1}$)
500	27	22
600	31	334
700	33	402

titania microparticles (20−60 μm). The compact shell shows well-replicated surface wrinkles, and the shell thickness is kept at ~2.6 μm for the hollow particles pyrolyzed at three different temperatures, indicating that the calcination temperature does not show remarkable effect on the shell thickness. The titania content in the titania/carbon composites was estimated through the TGA measurement performed in air, which shows that the titania content increases from 27 to 33 wt % with increasing calcination temperature from 500 to 700 °C (Table 1).

The XRD patterns of the hollow composite microparticles reveal that the calcination temperature exerts considerable influence on the crystallinity of titania. As shown in Figure 13, all the three titania/carbon composites exhibit relatively weak reflections corresponding to the anatase phase of titania along with a weak broad peak at ~10−30° attributed to

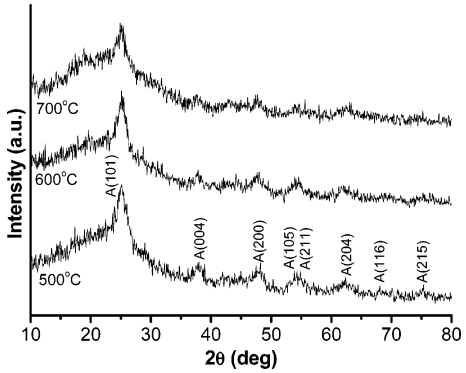

Figure 13. XRD patterns of hollow titania/carbon composite microparticles pyrolyzed in N_2 at different temperatures.

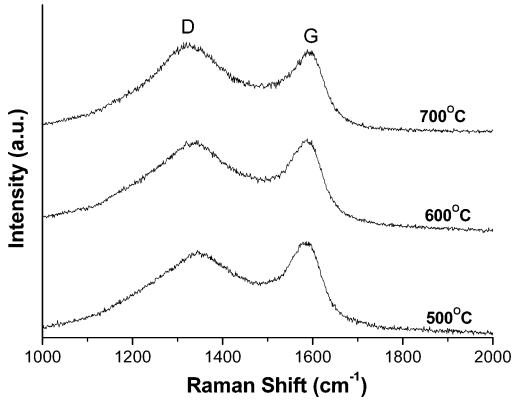

Figure 14. Raman spectra of hollow titania/carbon composite microparticles pyrolyzed in N_2 at different temperatures.

amorphous carbon. It can be seen that the crystallinity of anatase decreases with increasing calcination temperature, which may be rationalized by considering that the faster pyrolysis rate at a higher calcination temperature would lead to a faster incorporation of the poorly crystallized titania nanoparticles inside the pyrolyzing and shrinking dextran networks, favoring a stronger inhibition of the titania crystallization. It is noteworthy that while the phase transformation from anatase to rutile obviously occurred at 700 °C for the hollow titania microparticles (Figure 6), the rutile phase did not appear for the titania/carbon composites carbonized at 700 °C, suggesting that the phase transformation from anatase to rutile in titania/carbon composites can be effectively restrained, in good agreement with the previously reported results.[16] On the other hand, Raman spectra of the hollow composite microparticles have been measured to provide information about the nature of the carbon in the composites. As shown in Figure 14, the Raman spectra show two broad bands at 1350 and 1590 cm^{-1}, which are characteristic of a symmetry breakdown at the edge of graphene sheets (D band) and the E_{2g} vibrational mode of graphite layers (G band), respectively.[10c] The presence of both D and G bands is consistent with the model of turbostratically disordered graphene sheets contained in hard carbon, indicating that the carbon is disordered amorphous carbon,[10c,d] in accordance with the XRD result. It is noted that the D/G intensity ratio is slightly increased with increasing calcination temperature, suggesting that the carbon becomes a little more disordered for the titania/carbon composites carbonized at a higher temperature, which may

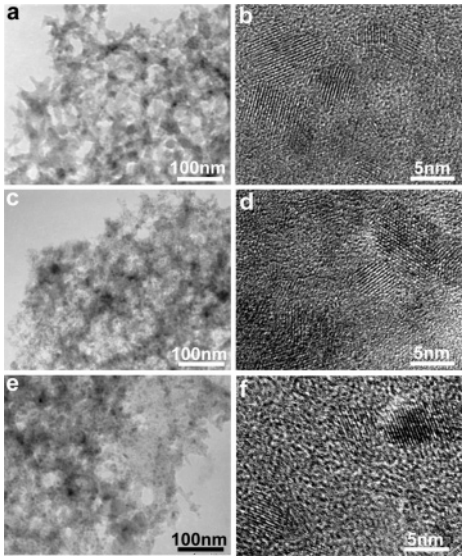

Figure 15. TEM (a, c, e) and HRTEM (b, d, f) images of hollow titania/carbon composite microparticles pyrolyzed in N_2 at different temperatures: (a, b) 500 °C, (c, d) 600 °C, and (e, f) 700 °C.

be also related with the faster pyrolysis rate at the higher calcination temperature.

TEM as well as HRTEM investigation has been carried out to reveal the microstructure of the hollow titania/carbon composite microparticles (Figure 15). The TEM image shown in Figure 15a shows that the titania/carbon composite pyrolyzed at 500 °C consists of interconnected networks with pore sizes larger than 10 nm, but it is difficult to discern individual titania nanocrystals. However, the related HRTEM image (Figure 15b) clearly shows the presence of many anatase nanocrystals (∼4−9 nm) randomly distributed in amorphous matrixes, that is, carbon networks. The titania/carbon composites pyrolyzed at higher temperatures (i.e., 600 and 700 °C) show microporous networks with much smaller pore sizes where anatase nanocrystals ∼5 nm are also randomly distributed (Figure 15c−f). The N_2 sorption measurement of the titania/carbon composite pyrolyzed at 600 °C showed that the single-point total pore volume at a relative pressure of 0.998 is 0.193 $cm^3\ g^{-1}$ with a micropore volume of 0.122 $cm^3\ g^{-1}$, indicating that the microporosity is predominant in this material. As shown in Table 1, the BET surface area of the titania/carbon composites pyrolyzed at 500 °C is as low as 22 $m^2\ g^{-1}$ whereas the composites pyrolyzed at 600 and 700 °C show much higher surface areas, that is, 334 $m^2\ g^{-1}$ and 402 $m^2\ g^{-1}$, respectively, which is consistent with the TEM observations. These results suggest that the carbonization at 500 °C is relatively slow and incomplete, resulting in partial preservation of the original network structure whereas the carbonization at higher temperatures is fast and approximately complete, resulting in the collapse of the original network structure and the formation of many new micropores.

The photocatalytic activity of the hollow titania/carbon composite microparticles was examined by measuring the photodegradation of Rhodamine B in an aqueous suspension of the titania/carbon composites with a concentration of 0.2 g L^{-1}. Considering that the porous carbon with a high surface area or adsorptivity may contribute to the apparent photo-

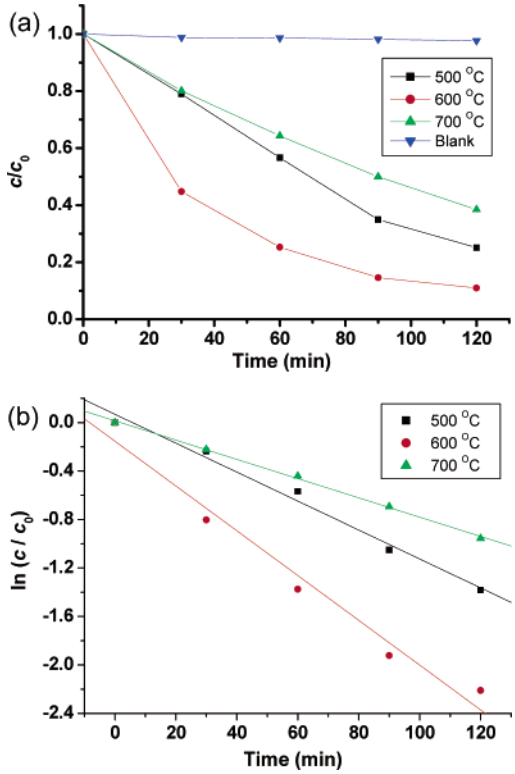

Figure 16. (a) Photodegradation of Rhodamine B monitored as the normalized concentration change versus irradiation time in the presence of hollow titania/carbon composite microparticles pyrolyzed in N_2 at different temperatures. (b) re-plot of part a as the linear graph of $\ln(c_0/c)$ vs time. The blank measurement was conducted without UV illumination in the presence the hollow titania/carbon composite microparticles pyrolyzed in N_2 at 700 °C.

catalytic activity through adsorption of Rhodamine B, a blank measurement was conducted without UV illumination in the presence the titania/carbon composite pyrolyzed at 700 °C. As shown in Figure 16a, there is almost no decrease in the Rhodamine B concentration after 2 h in the blank experiment, essentially excluding the contribution from the adsorption of Rhodamine B on the titania/carbon composites. It is shown that all three of the titania/carbon composites exhibit good photocatalytic activity with the titania/carbon composites pyrolyzed at the intermediate temperature (600 °C) showing the highest activity. The re-plotted linear graph of $\ln(c/c_0) \sim t$ shown in Figure 16b indicates that the photodegradation of Rhodamine B with the titania/carbon composites pyrolyzed at different temperatures follows roughly the pseudo-first-order reaction, which is consistent with results obtained from the photodegradation of Rhodamine B assisted by titania films.[30] The rate constants were determined to be 0.0119, 0.0185, and 0.0080 min^{-1} for the titania/carbon composites pyrolyzed at 500, 600, and 700 °C, respectively. This result may also be interpreted in terms of a compromise between the two important factors in determining the photocatalytic activity, that is, the crystallinity of anatase and the surface area of the hollow microparticles. In this case, the crystallinity of anatase decreases with increasing calcination temperature, and the surface area increases with increasing calcination temperature, in contrast to the case of hollow titania microparticles.

(30) Wu, J.-M.; Zhang, T.-W. *J. Photochem. Photobiol., A* **2004**, *162*, 171.

It is worth noting that the hollow titania/carbon composite microparticles pyrolyzed at 600 °C show a much better photocatalytic activity than all the hollow titania microparticles calcined at different temperatures even though the actual titania concentration in the suspension of the hollow composite microparticles is only 0.06 g L^{-1}, much smaller than the titania concentration in the suspension of hollow titania microparticles (0.1 g L^{-1}). Generally, this result may be attributed to the high photocatalytic activity related with titania/carbon composites, which have been previously reported for different types of titania/carbon composites and ascribed to several factors including stabilization of the anatase phase, increased surface area, and high adsorptivity of porous carbon.[15,16] Although the presence of a small amount of amorphous titania in the titania/carbon composites cannot be excluded, the amorphous titania is not expected to considerably contribute to the photodegredation reaction because amorphous titania is known to have negligible photocatalytic efficiency compared to that of the anatase phase.[20c] However, a more detailed understanding of the photocatalytic superiority of hollow titania/carbon composite microparticles over hollow titania microparticles is still underway. For comparison purposes, the photodegradation of Rhodamine B was performed in the presence of commercial Degussa P25 TiO_2, a reference photocatalyst. Under otherwise similar conditions, the rate constant for P25 was measured to be 0.0445 min^{-1}, which is still higher than that for all the obtained titania/carbon composites. This result is not unexpected because the current composite microspheres have much larger sizes compared with the powdered P25 nanoparticles. However, these titania/carbon composite microparticles have the advantage of being easy to handle and may be considered as a promising candidate for useful photocatalysts. Furthermore, it was found that the adsorptivity of the hollow titania/carbon composite microparticles was much higher than that of the hollow titania microparticles. For instance, the amount of Rhodamine B adsorbed onto the hollow microparticles after 30 min in the dark was measured to be 5.0×10^{-7} mol g^{-1} and 5.2×10^{-6} mol g^{-1} for the titania microparticles calcined at 500 °C and the titania/carbon composite microparticles pyrolyzed at 600 °C, respectively. Because the unique structure of micrometer-sized hollow particles and the novel properties of titania/carbon composites are combined together, the current hollow microparticles of titania/carbon composites may find many promising applications including as catalysts, adsorbents, electrode materials, and lightweight fillers. Compared with other approaches to fabricate hollow titania entities, the current approach is unique in that the commercial dextran gel beads were carbonized during the heating stage, resulting in novel hollow titania/carbon composite microparticles with dramatically enhanced photocatalytic activities.

Conclusions

A commercial cross-linked dextran gel, Sephadex G-100, has been successfully employed as the template for the controlled synthesis of hollow particles of titania and titania/carbon composites. The immersion of hollow Sephadex G-100 beads in aqueous $TiCl_4$ solution resulted in the gradual

deposition of titania on the surface of the gel networks, and hollow shrunken microparticles of titania/G-100 hybrids about 40−120 μm in size and ∼4.5 μm in shell thickness were obtained upon subsequent dehydrating and drying. Hollow titania microparticles about 20−60 μm in size were readily fabricated by calcination of the hollow titania/G-100 hybrid microparticles in air, and the shell thickness was adjusted from 1 to 2.5 μm through increasing the immersion reaction time from 2 to 24 h. An increase in the calcination temperature from 400 to 700 °C resulted in an increase in the crystallite size, which is accompanied by a phase transformation from anatase to rutile around 700 °C and a decrease in the surface area, while the apparent morphology of the hollow particles remains unchanged. The hollow titania microparticles calcined at 500 °C exhibited the highest photocatalytic activity because of a compromise between the anatase crystallinity and the surface area. For the synthesis of hollow microparticles of titania/carbon composites, the calcination of the hollow titania/G-100 hybrid microparticles was conducted at 500−700 °C in flowing N_2 to carbonize the cross-linked dextrans. The obtained hollow titania/carbon composite microparticles, which were about 30−90 μm in size and ∼ 2.6 μm in shell thickness, consisted of amorphous carbon and anatase nanocrystals, and the titania content was increased from 27 to 33 wt % with increasing the calcination temperature from 500 to 700 °C. The phase transformation from anatase to rutile at a calcination temperature of 700 °C was completely suppressed in the titania/carbon composites. Moreover, with increasing temperature from 500 to 700 °C, the crystallinity of anatase was decreased and the surface area was increased, in contrast to the case of hollow titania microparticles. All the obtained titania/carbon composites exhibit good photocatalytic activity with the titania/carbon composites pyrolyzed at 600 °C showing the highest activity possible as a result of a compromise between the crystallinity of anatase and the surface area of the hollow microparticles. Compared with the hollow titania microparticles, the hollow titania/carbon composite microparticles exhibit remarkably enhanced photocatalytic activity, which could be related to the characteristics of titania/carbon composites such as stabilization of the anatase phase, increased surface area, and high adsorptivity of porous carbon.

Considering the unique properties of the hollow particle structure, the obtained hollow microparticles of titania and titania/carbon composites may find many promising applications including as catalysts, adsorbents, electrode materials, and lightweight fillers. The templating synthesis based on Sephadex gels is potentially extendable to the synthesis of hollow microparticles of other metal oxide systems. Moreover, the size, shell thickness, microstructure, and chemical composition of the templated hollow microparticles could be adjusted through changing the properties of the Sephadex gel templates because Sephadex gels with tunable size and cross-linkage degree as well as Sephadex gels containing various functional groups are available. Therefore, the current templating synthesis strategy may represent a general method for the fabrication of inorganic hollow microparticles with tailored properties.

Acknowledgment. This work was supported by the National Natural Science Foundation of China (20325312, 20473003, 50521201, and 20233010) and the Foundation for the Author of National Excellent Doctoral Dissertation of China (200020).

CM060503P